The results of our molecular mechanics calculations on these square-planar isomers are shown in Table V; results from the previous calculations are also included for comparison.[26] In contrast to the latter results, the (low-spin) trans-III isomer was calculated to be the lower energy isomer in the present study, a result largely attributable to the presence of the out-of-plane bending term in the force field. That is, our calculations suggest that the trans-III isomer is favored over the trans-I isomer as originally proposed. While it remains difficult to decide on the "correct" order from the present study, the results do illustrate the sensitivity of the method to the nature of the force field employed.[56] Clearly, in studies of the present type, appropriate caution should be exercised when using the molecular mechanics procedure for predicting the relative energies of isomeric metal complexes.

Acknowledgment. We thank the Australian Institute of Nuclear Science and Engineering and the Australian Research Council for support.

(56) It needs to be emphasized that the present force field has been optimized only in terms of geometry and that the associated energy terms have not been "calibrated"—especially with respect to those parts of the structures influenced by the central metal.

The Pentafluoroxenate(IV) Anion, XeF_5^-: The First Example of a Pentagonal Planar AX_5 Species

Karl O. Christe,*[1] Earl C. Curtis,[1] David A. Dixon,[2] Hélène P. Mercier,[3] Jeremy C. P. Sanders,[3] and Gary J. Schrobilgen*[3]

Contribution from Rocketdyne, A Division of Rockwell International, Canoga Park, California 91303, the Department of Chemistry, McMaster University, Hamilton, Ontario L8S 4M1, Canada, and the Central Research and Development Department, E. I. du Pont de Nemours and Company, Inc., Experimental Station, Wilmington, Delaware 19880-0328. *Received September 28, 1990*

Abstract: Xenon tetrafluoride forms stable 1:1 adducts with $N(CH_3)_4F$, CsF, RbF, KF, and NaF and an unstable 1:1 adduct with FNO. All these adducts are ionic salts containing pentagonal planar XeF_5^- anions as shown by a crystal structure determination of $N(CH_3)_4^+XeF_5^-$, Raman and infrared spectra, and ^{19}F and ^{129}Xe NMR spectroscopy. The X-ray crystal structure of $N(CH_3)_4^+XeF_5^-$ was determined at −86 °C. This compound crystallizes in the orthorhombic system, space group *Pmcn*, with four molecules in a unit cell of dimensions a = 6.340 (2) Å, b = 10.244 (3) Å, and c = 13.896 (4) Å with R = 0.0435 for 638 observed [$I > 3\sigma(I)$] reflections. In addition to four $N(CH_3)_4^+$ cations, the structure contains four pentagonal planar XeF_5^- anions per unit cell with D_{5h} symmetry. The Xe–F distances are 1.979 (2)–2.034 (2) Å with F–Xe–F angles of 71.5 (4)–72.3 (4)°. The D_{5h} structure of the XeF_5^- anion is highly unusual and represents the first example of an AX_5E_2 (E = valence electron lone pair) species in which all six atoms are coplanar. The results from the crystal structure determination and a normal coordinate analysis show that the XeF_5 plane of XeF_5^- is considerably more rigid than that in the fluxional IF_7 molecule due to the increased repulsion from the xenon free valence electron pairs. Local density functional calculations were carried out for XeF_5^- and XeF_4 with a double-numerical basis set augmented by polarization functions and confirm the experimentally observed geometries and vibrational spectra. It is shown that the bonding in XeF_5^- closely resembles that in XeF_4. In a valence bond description, it can be visualized as the two axial positions being occupied by two sp-hybridized free valence electron pairs and the equatorial fluorines being bound by two Xe 5p electron pairs through semiionic multicenter four-electron bonds.

Introduction

Recent work in our laboratories has shown that anhydrous $N(CH_3)_4F$[4] holds great potential for the synthesis and characterization of novel, high oxidation state, complex fluoro anions.[5-7] An area of special interest to us is the problem of maximum coordination numbers and their influence on the steric activity of free valence electron pairs. For example, it was shown that nitrogen(V) cannot accommodate five fluorine ligands,[8] whereas the iodine in IF_6^-, which had long been thought to have a distorted octahedral structure,[9,10] has recently been confirmed to possess a sterically active lone valence electron pair.[10] In contrast, the central atom free valence electron pairs in the smaller ClF_6^- and BrF_6^- anions become sterically inactive due to space limitations, as demonstrated in very recent vibrational[6,10] and single-crystal X-ray structure studies.[11]

In this context, the likely structures of the XeF_5^- and XeF_6^{2-} anions posed an interesting problem, since both anions contain two free valence electron pairs on the xenon central atom. Therefore, they are representatives of the novel AX_5E_2 and AX_6E_2 geometries, respectively, where E stands for a free valence electron pair. Whereas no reports have been published on the existence or possible structure of XeF_5^- or any other AX_5E_2 species, Kiselev and co-workers[13-15] recently reported the synthesis of M_2XeF_6 salts (M = Cs, Rb, K, Na) from XeF_4 and MF. On the basis of vibrational spectra, they surprisingly assigned an octahedral structure to XeF_6^{2-}. However, a closer inspection of their published

(1) Rockwell International, Rocketdyne Division.
(2) E. I. du Pont de Nemours and Company, Inc.
(3) McMaster University.
(4) Christe, K. O.; Wilson, W. W.; Wilson, R. D.; Bau, R.; Feng, J. *J. Am. Chem. Soc.* **1990**, *112*, 7619.
(5) Wilson, W. W.; Christe, K. O. *Inorg. Chem.* **1989**, *28*, 4172.
(6) Christe, K. O.; Wilson, W. W.; Chirakal, R. V.; Sanders, J. C. P.; Schrobilgen, G. J. *Inorg. Chem.* **1990**, *29*, 3506.
(7) Wilson, W. W.; Christe, K. O.; Feng, J.; Bau, R. *Can. J. Chem.* **1989**, *67*, 1988.
(8) Christe, K. O.; Wilson, W. W.; Schrobilgen, G. J.; Chirakal, R. V.; Olah, G. A. *Inorg. Chem.* **1988**, *27*, 789.
(9) Klamm, H.; Meinert, H.; Reich, P.; Witke, P. *Z. Chem.* **1968**, *8*, 469.
(10) Christe, K. O.; Wilson, W. W. *Inorg. Chem.* **1989**, *28*, 3275 and references cited therein.
(11) Mahjoub, A. R.; Hoser, A.; Fuchs, J.; Seppelt, K. *Angew. Chem., Int. Ed. Engl.* **1989**, *28*, 1526.
(12) Reference deleted in proof.
(13) Spitzin, V. I.; Kiselev, Yu. M.; Fadeeva, N. E.; Popov, A. I.; Tchumaevsky, N. A. *Z. Anorg. Allg. Chem.* **1988**, *559*, 171.
(14) Kiselev, Yu. M.; Goryachenkov, S. A.; Martynenko, L. I.; Spitsyn, V. I. *Dokl. Akad. Nauk SSSR* **1984**, *278*, 881.
(15) Kiselev, Yu. M.; Fadeeva, N. E.; Popov, A. I.; Korobov, M. V.; Nikulin, V. V.; Spitsyn, V. I. *Dokl. Akad. Nauk SSSR* **1987**, *295*, 378.

0002-7863/91/1513-3351$02.50/0

spectra[13] revealed that both the frequency separations and relative intensities of the observed bands are incompatible with an octahedral species.[16] Furthermore, it was noted that the Raman spectrum attributed to Cs_2XeF_6 was identical with that previously observed during the laser photolysis of $CsXeF_7$ and tentatively assigned to Cs_2XeF_8.[17] In view of these discrepancies we decided to investigate the fluoride-acceptor properties of XeF_4 using $N(CH_3)_4F$ as a fluoride ion source and to reinvestigate the XeF_4–MF systems.

Experimental Section

Apparatus and Materials. Volatile materials were handled in stainless steel–Teflon and Pyrex glass vacuum lines, as previously described.[18,19] Nonvolatile materials were handled in the dry nitrogen atmosphere of a glovebox.

Literature methods were used for the syntheses of anhydrous $N(CH_3)_4F$,[4] XeF_4,[20] and FNO[21] and the drying of CH_3CN.[4,22] The LiF (Research Inorganic Chemicals, Research Organic Chemicals), NaF (Matheson), and BaF_2 (Baker and Adamson) were dried under vacuum at 125 °C prior to their use. The KF (Allied), RbF (American Potash), and CsF (KBI) were dried by fusion in a platinum crucible, followed by transfer of the hot clinkers to the dry nitrogen atmosphere of the glovebox where the fluoride samples were ground prior to use.

Syntheses of $M^+XeF_5^-$ (M = Cs, Rb, K, Na). The dry, finely powdered alkali metal fluorides (2 mmol) and XeF_4 (4–8 mmol) were loaded inside the drybox into prepassivated (with ClF_3), 10-mL, stainless steel Hoke cylinders that were closed by metal valves. The cylinders were evacuated at −78 °C on the vacuum line and then heated in an oven to 190 °C for 14 h. Unreacted XeF_4 was pumped off at 30 °C and collected in a tared Teflon U-trap at −196 °C until the cylinders reached a constant weight. The combining ratios of MF with XeF_4 were obtained from the observed material balances, i.e., the weights of MF, XeF_4 used, XeF_4 recovered, and the products. Under the above conditions, the following combining ratios were observed: CsF:XeF_4 = 1:0.99, RbF:XeF_4 = 1:0.95, KF:XeF_4 = 1:0.65, and NaF:XeF_4 = 1:0.32. Additional heating of the KF–XeF_4 and NaF–XeF_4 adducts with more XeF_4 to 135 °C for 10 days increased the conversion of KF and NaF to the corresponding XeF_5^- salts to 73% and 36%, respectively.

Synthesis of $NO^+XeF_5^-$. In the drybox, XeF_4 (1.03 mmol) was loaded into a prepassivated 0.5-in.-o.d. Teflon–FEP ampule that was closed by a stainless steel valve. On the vacuum line, FNO (6.77 mmol) was added to the ampule at −196 °C. The ampule was allowed to warm to 0 °C and was kept at this temperature for 10 min with agitation, and the unreacted FNO was then pumped off at −78 °C. The white solid residue (265 mg, weight calculated for 1.03 mmol of $NO^+XeF_5^-$ = 264 mg) had a dissociation pressure of 10 Torr at 0 °C.

Synthesis of $N(CH_3)_4^+XeF_5^-$. In a typical synthesis, $N(CH_3)_4F$ and XeF_4 (2.01 mmol each) were loaded into a Teflon–FEP ampule in a drybox and CH_3CN (3 mL liquid) was vacuum distilled onto the solid at −196 °C. The mixture was warmed to −40 °C for 30 min with agitation and then allowed to warm to room temperature, followed by removal of the solvent in vacuo at this temperature. The white solid residue [605 mg, weight calculated for 2.01 mmol of $N(CH_3)_4^+XeF_5^-$ = 604 mg] was identified as $N(CH_3)_4^+XeF_5^-$ by vibrational and NMR spectroscopy and a crystal structure determination. When isolated from CH_3CN solution, the compound is stable indefinitely at room temperature.

Caution! When solutions of $N(CH_3)_4^+XeF_5^-$ in CH_3CN are frozen in liquid nitrogen, they may detonate. Similar, but milder, detonations were also found to occur when XeF_4 solutions were frozen at −196 °C. Exposure of solid samples of $N(CH_3)_4^+XeF_5^-$ to atmospheric moisture for even brief periods has resulted in the violent detonation of bulk samples.

Crystal Structure Determination of $N(CH_3)_4^+XeF_5^-$. Crystal Growing. Single crystals of $N(CH_3)_4^+XeF_5^-$ suitable for X-ray analysis were grown from CH_3CN solution by vacuum distilling ca. 2.5 mL of dry CH_3CN onto ca. 50 mg of $N(CH_3)_3^+XeF_5^-$ in a $^1/_4$-in.-o.d. FEP reaction vessel equipped with a Kel-F valve. The mixture was warmed to 65 °C to effect dissolution and allowed to cool slowly to room temperature (ca. 5 °C/h). Colorless crystals up to 5 mm in length, having a needle-like morphology, formed overnight. The mother liquor was syringed off the crystals in a dry nitrogen atmosphere and residual solvent was removed under dynamic vacuum. Several crystals were cleaved perpendicular to their long axes to give fragments measuring ca. 0.2 mm × 0.2–0.3 mm and transferred in a drybox to 0.2-mm-o.d. Lindemann glass capillaries (previously dried under dynamic vacuum at 250 °C for 1 day) and sealed under a dry nitrogen atmosphere. The crystals were shown to be identical with the bulk sample prior to recrystallization by obtaining the single-crystal Raman spectrum at room temperature (see Figure 5b) and were found to be stable at room temperature in glass indefinitely.

Table I. Summary of Crystal Data and Refinement Results for $[N(CH_3)_4]^+[XeF_5]^-$[a]

space group	*Pmcn* (orthorhombic)
a (Å)	6.340 (2)
b (Å)	10.244 (3)
c (Å)	13.896 (4)
V (Å^3)	902.55
molecules/unit cell	4
molec wt (g mol^{-1})	300.44
calcd density (g cm^{-3})	2.153
T (°C)	−86
color	colorless
cryst decay (%)	0.6
μ (cm^{-1})	35.77
wavelength (Å) used for data collectn	0.710 69
sin θ/λ limit (Å^{-1})	0.538
total no. of reflcns measured	1414
no. of independent reflcns	641
no. of reflcns used in struct anal. $I > 3\sigma(I)$	638
no. of variable params	83
final agreement factors	R(F) = 0.0435 R(WF) = 0.0435

[a] Unit cell parameters obtained at 23 °C were a = 6.400 Å, b = 10.321 Å, and c = 14.029 Å; volume, 926.71 Å^3.

Collection and Reduction of X-ray Data. Crystals of $N(CH_3)_4^+XeF_5^-$ were centered on a Syntex P_3 diffractometer. Accurate cell dimensions were determined at T = 23 °C and at T = −86 °C from a least-squares refinement of the setting angles (χ, φ, and 2θ) obtained from 15 accurately centered reflections (with 22.14° < 2θ < 28.11°) chosen from a variety of points in reciprocal space. At T = 23 °C, and after several hours in the X-ray beam, the crystal appeared to be totally decomposed, resulting in an opaque white coloration. Integrated diffraction intensities were collected on a new crystal at T = −86 °C using a θ–2θ scan technique (slowest rate 5.0°/min) with $0 \le h \le 10$, $0 \le k \le 15$, and $-15 \le l \le 15$, using molybdenum radiation monochromatized with a graphite crystal (λ = 0.710 69 Å). Throughout the data collection, two standard reflections were monitored every 48 reflections; a decay of 0.6% was observed; the intensities were adjusted accordingly. A total of 1414 reflections were collected out of which 641 reflections, satisfying the condition $I > 3\sigma(I)$, were chosen for structure solution. The intensities of these reflections were corrected for Lorentz polarization effects.

Solution and Refinement of the Structure. There were two space groups that were consistent with the reflection pattern: the noncentrosymmetric space group $P2_1cn$ (No. 33) and the centrosymmetric space group *Pmcn* (No. 62). The structure has been solved in both centrosymmetric (*Pmcn*) and noncentrosymmetric ($P2_1cn$) space groups. The direct method of structure solution in the computer program SHELX-76[23] was used to locate the positions of the Xe atom and the five F atoms. Successive Fourier synthesis yielded all the remaining non-hydrogen atoms. The structure was refined by using the full-matrix least-squares technique with isotropic thermal parameters for individual atoms. In the case of the *Pmcn* space group and after full convergence of the isotropic refinement (R = 0.1265), the atoms were assigned anisotropic thermal parameters and further refined by the full-matrix least-squares technique (R = 0.0714). The positions of the hydrogen atoms were calculated and the fixed hydrogen atoms were given an isotropic temperature factor of 0.05 Å^2.[24] The R factor obtained was 0.0652, with the unit weights. There was significant disagreement between the F_o and F_c values of three reflections, 110, 312, and 413, and these values were consequently omitted in a further refinement. This resulted in a global improvement of the structure and a final value for the R factor of 0.0435.

(16) Weidlein, J.; Müller, U.; Dehnicke, K. *Schwingungsspektroskopie*; Georg Thieme Verlag: Stuttgart, Germany, 1982.
(17) Christe, K. O.; Wilson, W. W. *Inorg. Chem.* **1982**, *21*, 4113.
(18) Christe, K. O.; Wilson, R. B.; Schack, C. J. *Inorg. Synth.* **1986**, *24*, 3.
(19) Syvret, R. G.; Schrobilgen, G. J. *Inorg. Chem.* **1989**, *28*, 1564.
(20) (a) Bartlett, N.; Sladky, F. O. *J. Am. Chem. Soc.* **1968**, *90*, 5316. (b) Malm, J. G.; Chernick, C. L. *Inorg. Synth.* **1966**, *8*, 254.
(21) Christe, K. O. *Inorg. Chem.* **1972**, *12*, 1580.
(22) Winfield, J. M. *J. Fluorine Chem.* **1984**, *25*, 91.
(23) Sheldrick, G. M. *SHELX-76 Program for Crystal Structure Determination*; University of Cambridge: Cambridge, England, 1976.
(24) Hall, S. R.; Stewart, J. H. *XTAL 2.6 User's Manual*; University of Western Australia and University of Maryland.

Table II. Final Atomic Coordinates for $[N(CH_3)_4]^+[XeF_5]^-$

atom	x	y	z	pop.[a]
Xe1	0.2500	0.1233 (1)	0.0155 (1)	0.5
F1	0.2500	0.1876 (9)	0.1497 (6)	0.5
F2	0.2500	−0.0324 (8)	0.1025 (6)	0.5
F3	0.2500	−0.0399 (8)	−0.0673 (6)	0.5
F4	0.2500	0.1799 (9)	−0.1236 (6)	0.5
F5	0.2500	0.3217 (8)	0.0110 (6)	0.5
N1	0.2500	−0.403 (1)	0.172 (1)	0.5
C1	0.2500	0.628 (2)	0.068 (1)	0.5
C2	0.2500	−0.281 (2)	0.231 (1)	0.5
C3	0.437 (5)	−0.483 (2)	0.196 (1)	1.0

[a] The site occupation factor.

The same procedure was used for the *P21cn* space group, which gave rise to a final *R* factor of 0.0763. The ratio of agreement factors *R*-(7.63/4.35) = 1.75 is sufficient by Hamilton's *R* factor ratio test[7] to state that the correct space group is *Pmcn*.

An empirical absorption correction was also applied, but no significant improvement in the refinement was observed; in particular there was no change in the anisotropic thermal parameters.

Details of the data collection parameters and other crystallographic information for the *Pmcn* space group are given in Table I, and the final atomic coordinates are summarized in Table II. The following programs were used: XTAL,[24] data reduction; SHELX-76,[23] structure refinement; SNOOPI,[25] diagrams.

Vibrational Spectroscopy. Raman spectra were recorded on either a Cary Model 83 or a Spex Model 1403 spectrophotometer using a 488-nm exciting line of an Ar ion or the 647.1-nm line of a Kr ion laser, respectively. Baked-out Pyrex melting point capillaries or thin-walled Kel-F tubes were used as sample containers. A previously described[26] device was used for recording the low-temperature spectra (at −150 °C). Single-crystal spectra of $N(CH_3)_4^+XeF_5^-$ were recorded at room temperature on a Instruments S.A. Mole S-3000 triple spectrograph system equipped with a microscope for focusing the excitation laser to a one-micrometer spot. The Ar laser line at 514.5 nm was selected for excitation of the sample. Crystals were sealed in Lindemann glass capillaries as described below.

Infrared spectra were recorded by using AgBr disks on a Perkin-Elmer Model 283 spectrophotometer. The finely powdered samples were sandwiched between two thin AgBr disks and pressed together in a Wilks minipress inside the drybox.

Nuclear Magnetic Resonance Spectroscopy. The ^{19}F and ^{129}Xe NMR spectra were recorded unlocked (field drift < 0.1 Hz h^{-1}) with Bruker WM-250 and Bruker AM-500 spectrometers equipped with 5.8719-T and 11.744-T cryomagnets, respectively. Fluorine-19 spectra were obtained by using a 5-mm combination $^1H/^{19}F$ probe operating at 235.36 MHz. The spectra were accumulated in 16K memory. Spectral width settings of 5000 and 30 000 Hz were employed, yielding data point resolutions of 0.61 and 3.6 Hz/data point and acquisition times of 1.638 and 0.279 s, respectively. No relaxation delays were applied. Typically 300–7000 transients were accumulated. The pulse width corresponding to a bulk magnetization tip angle, θ, of approximately 90° was equal to 1 μs. No line broadening parameters were applied in the exponential multiplication of the free induction decays prior to Fourier transformation.

Xenon-129 NMR spectra were obtained by using a broad-band VSP probe tunable over the range 23–202 MHz; spectra were recorded at 139.05 MHz. The spectra were accumulated in a 16K memory. A spectral width setting of 50 kHz was employed, yielding a data point resolution of 6.1 Hz/data point and an acquisition time of 0.164 s. No relaxation delays were applied. Typically 10 000 transients were accumulated. The pulse width corresponding to a bulk magnetization tip angle, θ, of approximately 90° was equal to 18 μs. Line-broadening parameters of 4 Hz were applied in the exponential multiplication of the free induction decays prior to Fourier transformation.

The ^{19}F and ^{129}Xe NMR spectra were referenced to neat external samples of $CFCl_3$ and $XeOF_4$, respectively, at ambient temperature. The chemical shift convention used is that a positive (negative) sign signifies a chemical shift to high (low) frequency of the reference compound.

The ^{129}Xe NMR samples of saturated solutions of $N(CH_3)_4^+XeF_5^-$ in CH_3CN were prepared in 25-cm lengths of $^3/_8$-in.-o.d., $^1/_{32}$-in. wall FEP plastic tubing that had been reduced to 9-mm o.d. by squeezing in a heated precision brass mold. The FEP tubing was heat sealed at one end with the open end flared (45° SAE) and joined, by means of compression fittings, to a Kel-F valve. The FEP tubes were heat sealed under dynamic vacuum with their contents frozen at −78 °C. The sealed FEP sample tubes were inserted into 10-mm thin-walled precision NMR tubes (Wilmad) in order to run their spectra.

The ^{19}F NMR samples were prepared in precision 5-mm glass NMR tubes (Wilmad). Solid $N(CH_3)_4^+XeF_5^-$ [or $N(CH_3)_4^+XeF_5^-$ and $N(CH_3)_4^+F^-$] was loaded into the NMR tube in the drybox and CH_3CN solvent distilled in vacuo into the tube at −78 °C. The tube was flame sealed. On warming to room temperature, a colorless saturated solution resulted containing some solid $N(CH_3)_4^+XeF_5^-$, which was decanted into the top of the tube prior to obtaining the NMR spectrum.

Computational Method. The calculations described below were done by using the local density functional theory[27-30] with the program system DMol.[31] DMol employs numerical functions for the atomic basis sets. The atomic basis functions are given numerically as an atom-centered, spherical, polar mesh. The radial portion of the grid is obtained from the solution of the atomic LDF equations by numerical methods. The radial functions are stored as sets of cubic spline coefficients so that the radial functions are piecewise analytic, a necessity for the evaluation of gradients. The use of exact spherical atom results offers certain advantages. Because of the quality of the atomic basis sets, basis set superposition effects should be minimized, correct behavior at the nucleus is obtained, and radial nodal properties of the wave function are present.

Because the basis sets are numerical, the various integrals arising from the expression for the energy need to be evaluated over a grid. The integration points are generated in terms of angular functions and spherical harmonics. The number of radial points N_R is given as

$$N_R = 1.2 \times 14(Z + 2)^{1/3} \quad (1)$$

where Z is the atomic number. The maximum distance for any function is 12 au. The angular integration points N_0 are generated at the N_R radial points to form shells around each nucleus. The value of N_0 ranges from 14 to 302 depending on the behavior of the density.[32] The Coulomb potential corresponding to the electron repulsion term could be solved by evaluation of integrals. However, since the method is based on the density, it was found to be more appropriate to determine the Coulomb potential directly from the electron density by solving Poisson's equation

$$-\nabla^2 V_e(r) = 4\pi e^2 \rho(r) \quad (2)$$

In DMol, the form for the exchange–correlation energy of the uniform electron gas is that derived by von Barth and Hedin.[33]

All of the DMol calculations were done with a double-numerical basis set augmented by *d* polarization functions. This can be thought of in terms of size as a polarized double-ζ basis set. However, because exact numerical solutions are employed for the atom, this basis set is of significantly higher quality than a normal molecular orbital polarized double-ζ basis set. The fitting functions have an angular momentum number one greater than that of the polarization function, resulting in a value of $l = 3$ for the fitting functions.

Geometries were determined by optimization using analytic gradient methods.[34] First derivatives in the LDF framework can be calculated efficiently and only take on the order of three to four SCF iterations or 10–25% of an energy evaluation. There are two problems with evaluating gradients in the LDF framework, which are due to the numerical methods that are used. The first is that the energy minimum does not nec-

(25) Davies, K. *CHEMGRAF Suite: SNOOPI*; Chemical Design Ltd.: Oxford, England, 1983.
(26) Miller, F. A.; Harney, B. M. *Appl. Spectrosc.* **1969**, *23*, 8.
(27) Parr, R. G.; Yang, W. *Density Functional Theory of Atoms and Molecules*; Oxford University Press: New York, 1989.
(28) Salahub, D. R. In *Ab Initio Methods in Quantum Methods in Quantum Chemistry*, 2nd ed.; Lawley, K. P., Ed.; J. Wiley & Sons: New York, 1987; p 447.
(29) (a) Wimmer, E.; Freeman, A. J.; Fu, C.-L.; Cao, P.-L.; Chou, S.-H.; Delley, B. In *Supercomputer Research in Chemistry and Chemical Engineering*; Jensen, K. F., Truhlar, D. G., Eds.; ACS Symposium Series: American Chemical Society: Washington, DC, 1987; p 49. (b) Dixon, D. A.; Andzelm, J.; Fitzgerald, G.; Wimmer, E.; Delley, B. In *Science and Engineering on Cray Supercomputers. Proceedings of the Fifth International Symposium*; Cray Research: Minneapolis, MN, 1990; p 285.
(30) Jones, R. O.; Gunnarsson, O. *Rev. Mod. Phys.* **1989**, *61*, 689.
(31) Delley, B. *J. Chem. Phys.* **1990**, *92*, 508. DMol is available commercially from BIOSYM Technologies, San Diego, CA.
(32) This grid can be obtained by using the FINE parameter in DMol.
(33) von Barth, U.; Hedin, L. *J. Phys. Chem.* **1972**, *5*, 1629.
(34) (a) Versluis, I.; Ziegler, T. *J. Chem. Phys.* **1988**, *88*, 3322. (b) Andzelm, J.; Wimmer, E.; Salahub, D. R. In *The Challenge of d and f Electrons: Theory and Computation*; Salahub, D. R., Zerner, M. C., Eds.; ACS Symposium Series 394; American Chemical Society: Washington, DC, 1989; p 228. (c) Fournier, R.; Andzelm, J.; Salahub, D. R. *J. Chem. Phys.* **1989**, *90*, 6371.
(35) Pauling, L. *The Nature of the Chemical Bond*, 3rd ed.; Cornell University Press: Ithaca, NY, 1960; p 260.
(36) Bondi, A. J. *Phys. Chem.* **1964**, *68*, 441.

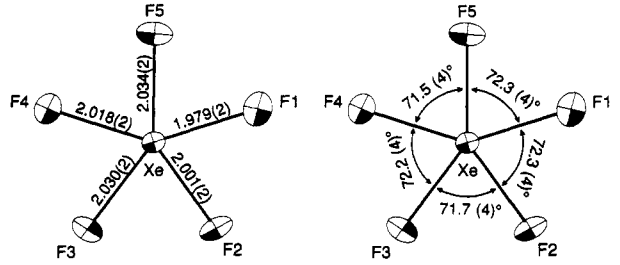

Figure 1. Atom numbering scheme, bond lengths (Å) and angles (deg) for XeF_5^- at −86 °C in $[N(CH_3)_4]^+[XeF_5]^-$. Projection of the XeF_5^- anion on (111). Esd's are given in parentheses; thermal ellipsoids are shown at the 50% probability level.

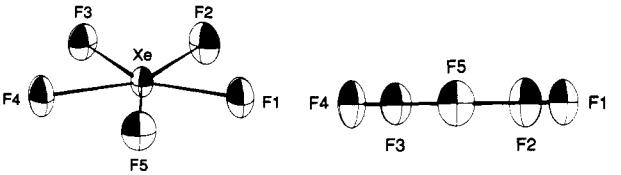

Figure 2. Projections of the XeF_5^- anion on (130) (left) and (010) (right). Thermal ellipsoids are shown at the 50% probability level.

essarily correspond exactly to the point with a zero derivative. The second is that sum of the gradients may not always be zero as required for translational invariance. These tend to introduce errors on the order of 0.001 Å in the calculation of the coordinates if both a reasonable grid and basis set are used. This gives bond lengths and angles with reasonable error limits. The difference of 0.001 Å is about an order of magnitude smaller than the accuracy of the LDF geometries as compared to experiment.

Results and Discussion

Syntheses and Properties of XeF_5^- Salts. The reactions of the alkali-metal fluorides with XeF_4 were studied under conditions (190 °C, 14 h) very similar to those previously reported by Kiselev and co-workers.[13-15] It was found that XeF_4 combines with either CsF or RbF in a clean 1:1 mole ratio to form the corresponding, previously unidentified XeF_5^- salts. In the case of KF and NaF the same anion was formed; however, the percentage conversion of MF to $MXeF_5$ decreased with decreasing atomic weight of M (CsF = 99%, RbF = 95%, KF = 65%, and NaF = 32%) and increased reaction times were required for higher conversions.

The interactions of LiF and BaF_2 with XeF_4 were also examined, but in neither case was evidence for the formation of a stable adduct obtained.

The XeF_5^- salts of Cs^+, Rb^+, K^+, and Na^+ are white, stable solids. Their physical properties, thermal stabilities, etc. are those previously attributed by Kiselev and co-workers to the corresponding M_2XeF_6 salts.[13-15] As will be shown below, they all contain pentagonal planar XeF_5^- anions.

Attempts to prepare $CsXeF_5$ from CsF and XeF_4 at room temperature in CH_3CN solutions were unsuccessful because of the very low solubility of CsF in this solvent. However, the highly soluble $N(CH_3)_4F$ readily forms $N(CH_3)_4^+XeF_5^-$ under these conditions. Even with a 2:1 molar ratio of $N(CH_3)_4F$:XeF_4 in CH_3CN solvent and a large excess of MF in the XeF_4–MF systems, only XeF_5^-, and no XeF_6^{2-}, was observed, indicating that XeF_5^- is the favored anion. The $N(CH_3)_4^+XeF_5^-$ salt is a white, stable solid whose structure was established by a crystal structure determination and vibrational and NMR spectroscopy (see below).

Table III. Bond Distances (Å) and Bond Angles (deg) in $[N(CH_3)_4]^+[XeF_5]^-$

	Bond Lengths		
Xe1–F1	1.979 (2)	N1–C1	1.481 (6)
Xe1–F2	2.001 (2)	N1–C2	1.488 (6)
Xe1–F3	2.030 (2)	N1–C3	1.524 (4)
Xe1–F4	2.018 (2)		
Xe1–F5	2.034 (2)		
	Bond Angles		
F2–Xe1–F1	72.3 (4)	C2–N1–C1	110.7 (3)
F3–Xe1–F2	71.7 (4)	C3–N1–C1	108.9 (5)
F4–Xe1–F3	72.2 (4)	C3–N1–C2	109.6 (4)
F5–Xe1–F1	72.3 (4)		
F5–Xe1–F4	71.5 (4)		

The lack of XeF_6^{2-} formation in these systems was further demonstrated by a study of the FNO–XeF_4 system. Even when a large excess of FNO was used, only $NO^+XeF_5^-$, and no $(NO^+)_2XeF_6^{2-}$, was formed at temperatures as low as −78 °C. The $NO^+XeF_5^-$ salt is a white solid having a dissociation pressure of 10 Torr at 0 °C. It is ionic, containing NO^+ and XeF_5^- ions as shown by vibrational spectroscopy (see below).

In view of the above results and the structural evidence presented below, it appears quite clear that the salts obtained by the reactions of XeF_4 with fluoride ion sources are XeF_5^-, and not XeF_6^{2-}, salts. The fact that some of the products reported[13-15] by the Soviet workers gave elemental analyses approaching the M_2XeF_6 composition might be attributed to incomplete conversion of MF to $MXeF_5$ thus resulting in MF + $MXeF_5$. There is also no doubt that the products observed during the laser photolysis of either $CsXeF_7$ or NF_4XeF_7 were not XeF_8^{2-} but XeF_5^- salts.[17]

X-ray Crystal Structure of $N(CH_3)_4^+XeF_5^-$. The crystal structure consists of well-separated $N(CH_3)_4^+$ and XeF_5^- ions. The $N(CH_3)_4^+$ cation is tetrahedral with the expected bond lengths. Different views of the XeF_5^- anion are shown in Figures 1 and 2, while a stereoview of the packing in the unit cell is given in Figure 3 in which the hydrogen atoms have been omitted in the cation. Important bond lengths and angles are listed in Table III. The xenon and five fluorines of the XeF_5^- anion and the nitrogen and two carbons of the cation are located on special positions that are on the mirror plane, resulting in an anion that is planar by crystal symmetry. The closest anion–cation distance occurs between F2 and C2, which lies in the anion plane, at 3.105 (5) Å, whereas the remaining closest F···C distances occur at 3.237 (5) (F5···C1), 3.354 (5) (F3···C2), 3.370 (5) (F1···C3), and 3.651 (5) Å (F4···C2). The sum of the van der Waals radii of CH_3 (2.00 Å[35]) and F (1.35[35]–1.40[36] Å) is 3.35–3.40 Å. The F2···C2 distance suggests weak hydrogen bonding between the C2 methyl group and F2 and is somewhat shorter than the shortest F···C

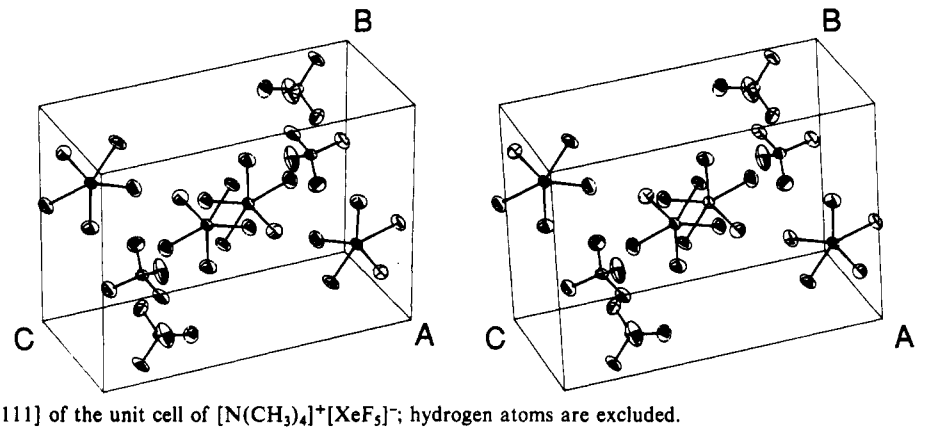

Figure 3. Stereoview [111] of the unit cell of $[N(CH_3)_4]^+[XeF_5]^-$; hydrogen atoms are excluded.

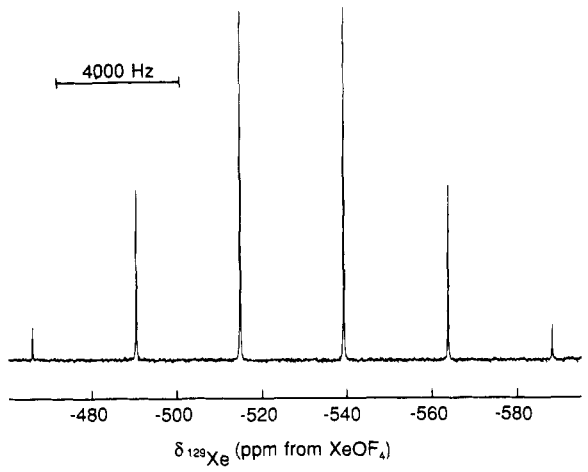

Figure 4. ^{129}Xe NMR spectrum (139.05 MHz) at 24 °C of a saturated solution of $N(CH_3)_4^+XeF_5^-$ in CH_3CN containing a 1 M excess of $N(CH_3)_4^+F^-$.

distance in $N(CH_3)_4^+HF_2^-$ [3.313 (5) Å],[7] which appears to be at the limit of the van der Waals distance. The short F2···C2 distance appears to account for the greater elongation of the thermal ellipsoid of F2 (in the direction of the C_5-axis of the anion; Figure 2).

Although the site symmetry of the XeF_5^- anion is C_s, the five fluorines are clearly equivalently bonded to the xenon, giving a pentagonal planar structure of D_{5h} symmetry. The average F–Xe–F angle of 72.0 (4)° is essentially the ideal angle of 72°. The average Xe–F bond length [2.012 (2) Å] is significantly longer than the average bond length of XeF_4 [1.953 (2) Å][37] and the average equatorial bond length of IF_7 [1.858 (4) Å].[38] The nearest-neighbor F···F contacts in the XeF_5^- anion are 2.35–2.38 Å and are substantially less than twice the nominal van der Waals radius for fluorine, i.e., 2.70[35]–2.80[38] Å, indicating that the fluorines of the pentagon are significantly congested and are consistent with the long Xe–F bond length in XeF_5^-. This contrasts with the shorter Xe–F bond length of XeF_4, where the fluorines in the plane are not contacting, and the intramolecular F···F distances (2.76 Å) are at the limit of the sum of the fluorine van der Waals radii. The short I–F bond lengths for the equatorial belt of five fluorines in IF_7 relative to the Xe–F bond length of XeF_5^- may be attributed to relief of the congestion in the IF_5 belt by means of a 7.5° puckering, which has been deduced from electron diffraction studies[38] but not corroborated by an independent study. The fact that XeF_5^- does not relieve its steric congestion by a puckering distortion may be attributed to the presence of the two axial lone pairs of electrons, which exert greater repulsive forces than the two axial fluorines in the IF_7 molecule, thus forcing the XeF_5^- anion to be planar. Moreover, the formal negative charge on XeF_5^- leads to a greater Xe–F bond polarity and elongation of the Xe–F bond, as is evident from a comparison with the Xe–F bond length of XeF_4, and serves to alleviate some of the steric congestion in the anion plane.

The steric crowding in the XeF_5^- molecular plane is further illustrated by the thermal parameters, which remain essentially unaltered before and after empirical absorption corrections. It is apparent that the principal axes of motion of the fluorine atoms in XeF_5^- and XeF_4[37] are perpendicular to the bond directions, producing the anticipated polar flattening of the thermal ellipsoids in the Xe–F bond directions. However, the thermal ellipsoids in XeF_5^- are elongated in the direction of the C_5-axis and flattened in the direction perpendicular to the Xe–F bonds in the molecular plane. In contrast to the fluorine thermal ellipsoids in XeF_5^-, those of XeF_4 are essentially isotropic in the directions perpendicular to the Xe–F bonds and in the molecular plane where the fluorine atoms are apparently not contacting one another to any significant

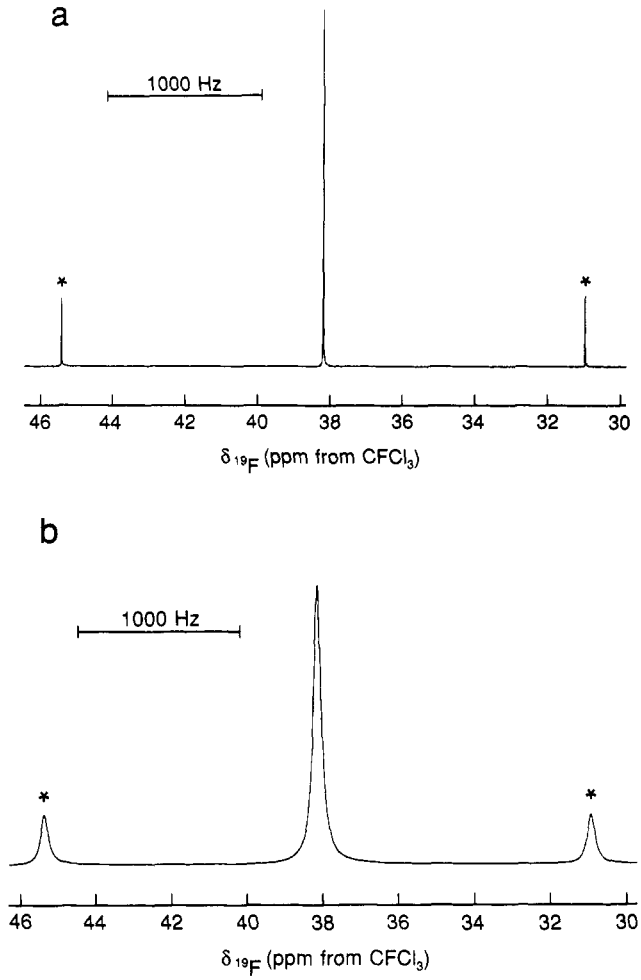

Figure 5. ^{19}F NMR spectrum (235.36 MHz) at 24 °C of (a) a saturated solution of $N(CH_3)_4^+XeF_5^-$ in CH_3CN containing a 1 M excess of $N(CH_3)_4^+F^-$ and (b) a saturated solution of pure $N(CH_3)_4^+XeF_5^-$ in CH_3CN. Asterisks (*) denote ^{129}Xe satellites.

extent. Steric congestion in XeF_5^- is additionally supported by vibrational force constant calculations (see below).

^{129}Xe and ^{19}F NMR Spectra of the XeF_5^- Anion. The ^{129}Xe NMR spectrum of $N(CH_3)_4^+XeF_5^-$ dissolved in CH_3CN containing a 1 M excess of $N(CH_3)_4^+F^-$ at 24 °C (Figure 4) displays a well-resolved binomial sextet ($\Delta\nu_{1/2}$ = 15 Hz), consistent with the coupling of the ^{129}Xe nucleus to five chemically equivalent ^{19}F nuclei in the XeF_5^- anion [$\delta(^{129}Xe)$, −527.0 ppm from $XeOF_4$; $^1J(^{129}Xe–^{19}F)$, 3400 Hz]. The ^{129}Xe chemical shift of XeF_5^- is significantly more shielded (i.e., by −843.9 ppm) than that of XeF_4 in CH_3CN at 24 °C [$\delta(^{129}Xe)$, 316.9 ppm from $XeOF_4$; $^1J(^{129}Xe–^{19}F)$, 3895 Hz]. This behavior follows the expected trend of increased shielding that accompanies an increase in negative charge.[39] The ^{19}F NMR spectrum of a similar sample at 24 °C (Figure 5a) shows a narrow singlet ($\Delta\nu_{1/2}$ = 2.8 Hz) flanked by natural abundance (26.44%) ^{129}Xe satellites [$\delta(^{19}F)$, 38.1 ppm from $CFCl_3$; $^1J(^{129}Xe–^{19}F)$, 3398 Hz]. A resonance due to unreacted fluoride was observed at −75 ppm. Interestingly, the ^{19}F chemical shift of XeF_5^- is deshielded by 56.8 ppm with respect to that of XeF_4 in CH_3CN at 24 °C [$\delta(^{19}F)$, −18.7 ppm from $CFCl_3$; $^1J(^{129}Xe–^{19}F)$, 3896 Hz]. This result is somewhat surprising in view of the increased ionic character of the Xe–F bonds (i.e., greater bond length and smaller stretching force constant) compared with those in XeF_4; the reason for this is not clear but may be related to the congested environment of the fluorine ligands and the rather short nearest-neighbor F···F contact distance. The ^{19}F NMR spectrum of a sample prepared from equimolar

(37) Burns, J. H.; Agron, P. A.; Levy, H. A. *Science* **1963**, *139*, 1208.
(38) Adams, W. J.; Thompson, H. B.; Bartell, L. S. *J. Chem. Phys.* **1970**, *53*, 4040.
(39) Jameson, C. J.; Mason, J. In *Multinuclear NMR*; Mason, J., Ed.; Plenum Press: New York, 1987; Chapter 3, pp 66–68.

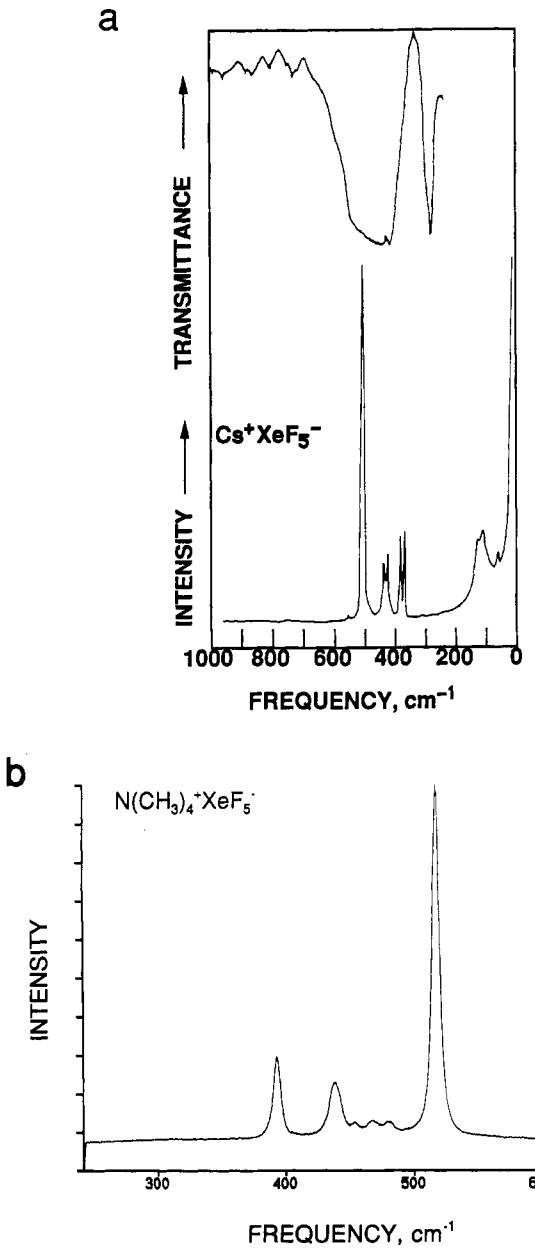

Figure 6. (a) Vibrational spectra of solid $Cs^+XeF_5^-$. Upper trace, infrared spectrum recorded at room temperature with an AgBr disk; lower trace; Raman spectrum recorded in a glass capillary at 25 °C with 647.1-nm excitation. (b) Single-crystal Raman spectrum of $N(CH_3)_4^+XeF_5^-$ recorded in a glass capillary at room temperature with 514.5-nm excitation.

quantities of XeF_4 and $N(CH_3)_4^+F^-$ in CH_3CN showed a similar resonance, with accompanying ^{129}Xe satellites, at 38.1 ppm; however, the linewidth was significantly broader, $\Delta\nu_{1/2}$ = 53 Hz (Figure 5b). This indicates that XeF_5^- undergoes dissociative fluorine exchange, which can be suppressed by the presence of excess fluoride. There was no evidence for the formation of XeF_6^{2-} at XeF_4:$N(CH_3)_4^+F^-$ ratios exceeding 1:1, thus casting further doubt on the previous claims[13-15] for the existence of stable salts of the XeF_6^{2-} anion.

The magnitude of the one-bond ^{129}Xe–^{19}F coupling constant drops from 3895 Hz in XeF_4 to 3400 Hz in XeF_5^- under the same conditions (i.e., solvent and temperature) of experimental measurement. If it is assumed that the Fermi-contact mechanism provides the dominant coupling contribution,[40] then the smaller

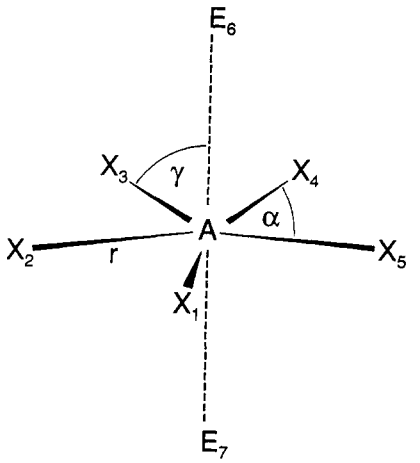

Figure 7. Internal coordinates for pentagonal planar AX_5.

value of $^1J(^{129}Xe–^{19}F)$ in XeF_5^- is in accord with the greater ionic character of the Xe–F bonds in the anion.

In the VSEPR notation, XeF_5^- is a seven-coordinate AX_5E_2 system, and is the first example of this geometry.[41] The solution structure proposed for the anion that is consistent with five equivalent fluorines is a pentagonal planar (D_{5h}) structure having five equivalent equatorial fluorines and two axial lone pairs of electrons. The dynamic behavior for related seven-coordinate geometries is well established in the cases of XeF_6 and IF_7. In contrast to IF_7 and XeF_5^-, the gas-phase structure of XeF_6 (AX_6E) is based upon a distorted octahedral geometry[42] in which the valence electron lone pair distorts the octahedral geometry to C_{3v} by occupying triangular faces of the octahedron, passing among adjacent faces via a transition state having intermediate C_s and C_{2v} geometries, with intramolecular exchange dynamics that are distinct from those of IF_7. The dynamic behavior of IF_7 (AX_7) is also well documented; on the basis of gas-phase electron diffraction measurements it is purported to have a puckered arrangement for the five equatorial fluorines[38] in the gas phase and it has been shown by ^{19}F NMR spectroscopy that axial and equatorial fluorine environments of IF_7 undergo rapid intramolecular exchange in solution.[43] The single fluorine environment observed in the NMR spectra of XeF_5^- could also be accounted for by assuming that the anion is fluxional. The VSEPR rules postulate that the valence shell lone pairs exert larger repulsive forces on adjacent electron pairs than do bonding pairs, so that, unlike IF_7, the transition state for exchange of axial lone pair positions with equatorial fluorine positions in XeF_5^- would presumably give rise to prohibitively large repulsive energies when a lone pair or lone pairs occupy an equatorial position, suggesting that XeF_5^- is likely to be rigid in solution.

Vibrational Spectra and Normal Coordinate Analysis of XeF_5^-. The infrared and Raman spectra of $CsXeF_5$, $RbXeF_5$, $KXeF_5$, $NaXeF_5$, and $N(CH_3)_4XeF_5$ and the Raman spectra of $NOXeF_5$ have been recorded. The observed frequencies and their assignments are summarized in Table IV. Figure 6 shows, as typical examples, the vibrational spectra of $CsXeF_5$ and $N(CH_3)_4XeF_5$.

As shown above by the NMR data and the crystal structure determination, the XeF_5^- anion is pentagonal planar and, therefore, belongs to point group D_{5h}. After the removal of translational and rotational degrees of freedom, the irreducible representation of the molecule is

$$\Gamma_{vib} = 1A_1'(R) + 1A_2''(IR) + 2E_1'(IR) + 2E_2'(R) + E_2''(ia)$$

Since XeF_5^- is the first known example of an AX_5 species of symmetry D_{5h}, it is not surprising that a normal coordinate analysis

(40) (a) Jameson, C. J. In *Multinuclear NMR*; Mason, J., Ed.; Plenum Press: New York, 1987; Chapter 4, pp 97–101; Chapter 18. (b) Schrobilgen, G. J. In *NMR and the Periodic Table*; Harris, R. K., Mann, B. E., Eds.; Academic Press: New York, 1978; Chapter 14.

(41) Gillespie, R. J. *Molecular Geometry*; Van Nostrand Reinhold Co.: London, 1972.

(42) (a) Bartell, L. S.; Gavin, R. M.; Thompson, H. B. *J. Chem. Phys.* **1965**, *43*, 2547. (b) Bartell, L. S.; Gavin, R. M. *J. Chem. Phys.* **1968**, *48*, 2466.

(43) Gillespie, R. J.; Quail, J. W. *Can. J. Chem.* **1964**, *42*, 2671.

Table IV. Vibrational Spectra of the XeF_5^- Anion in Different Salts

observed frequencies,[a] cm^{-1}												
$NOXeF_5$[b] R		$N(CH_3)_4XeF_5$[c]		$NaXeF_5$		$KXeF_5$		$RbXeF_5$		$CsXeF_5$		assignments for XeF_5^- in point group D_{5h}
25 °C	−150 °C	R	IR	R	IR	R	IR	R	IR	R	IR	
									970 vw		955 vw	$\nu_1 + \nu_3(E_1')$
									882 vw		870 sh	$\nu_3 + \nu_5(E_1' + E_2')$
							860 vw				850 vw	$2\nu_5(A_1' + E_1' + A_2')$
							800 vw		808 vw		795 vw	$\nu_5 + \nu_6(A_1' + E_1' + A_2')$
									752 vw		740 sh	$2\nu_6(A_1' + E_1')$
							740 vw		728 vw		724 vw, 705 sh	$\nu_4 + \nu_5(E_1' + E_2')$
									668 vw		650 sh	$\nu_4 + \nu_6(E_1' + E_2')$
						544 (0.1)		550 (0.1)		547 (0.1)		$2\nu_2(A_1')$
503 (10)	506 (10)	502 (10)		519 (10)	525 sh	505 (10)		509 (10)		504 (10)		$\nu_1(A_1')$
	498 (1)		509 sh			498 sh		489 sh				
482 (0+)			465 vs	473 (0.1)	450 vs, br		480 vs	471 (0.1)	470 vw, br		450 vs, br	$\nu_3(E_1')$
	475 (0.5)		420 sh		415 s		410 s	453 sh	418 s		415 s	
440 sh	445 (1.8)	423 (2.1)		444 (1.8)		438 (1.4)		440 (1.6)		432 (1.5)		$\nu_5(E_2')$
429 (1.1)	424 (1)			422 (1.3)		424 (1.2)		437 sh		422 (1.6)		
382 sh	384 (1)	377 (3.3)		386 (2.0)		388 (2.4)	379 sh	389 (2.2)	372 w	380 (2.2)		$\nu_6(E_2')$
374 (2.3)	373 (2.5)			383 sh		381 (1.9)		379 (1.6)		369 (2.3)		
290 (0+)	282 (0.5)			293 (0+)		290 (0+)		299 (0+)	288 sh	312 (0+)	288 sh	$\nu_4(E_1')$
240 (0.2)	244 (0.6)		278 s		276 s		275 s	278 (0+)	275 s		274 s	$\nu_2(A_2'')$
								169 (0.7)				
						147 (1.5)		131 (1.1)				
						113 sh		107 (0.4)				
135 (1)	144 (1.5)					102 (0.5)		91 (1.3)		124 (1.2)		
97 (0.8)	100 (1.5)	90 (1)		144 (1.4)		90 (2)		77 (1)		104 (1.5)		lattice vibrations
75 (1.5)	82 (3.0)					65 sh		59 (1.4)		57 (0.3)		
35 (0.5)	42 (1)					52 sh		52 sh				
						42 sh		47 sh				
								35 (0.6)				

[a] Values in parentheses denote relative intensities; sh, shoulder; s, strong; w, weak. [b] The NO^+ stretching mode was observed at 2314 cm^{-1} with a relative intensity of 1.0. [c] Only the bands due to the XeF_5^- anion have been listed in the table. In addition to these bands, the following bands due to the $N(CH_3)_4^+$ cation were observed. Ra: 3035 (0.2), 2990 (0.1), 2970 (0.1), 2930 (0.2), 2820 (0.1), 1484 (0.1), 1458 (0.3), 1185 (0+), 954 (0.5), 758 (0.9), 480 (0.2), 468 (0.2), 456 (0.1). IR: 3040 m, 2968 w, 1491 s, 1423 w, 954 s, 462 s. For their assignment, see ref 3.

Table V. Symmetry Coordinates and Approximate Mode Descriptions for a Pentagonal Planar XY_5 Molecule

$S_1 = \frac{1}{\sqrt{5}}(\Delta r_1 + \Delta r_2 + \Delta r_3 + \Delta r_4 + \Delta r_5)$	symmetric stretch
$S_2 = \frac{1}{\sqrt{10}}[\sum_{i=1}^{5}(\Delta\gamma_{i6} - \Delta\gamma_{i7})]$	symmetric out of plane (umbrella) deformation
$S_{3a} = \sqrt{\frac{2}{5}}[\Delta r_1 + \cos\alpha(\Delta r_2 + \Delta r_5) + \cos 2\alpha(\Delta r_3 + \Delta r_4)]$	asymmetric stretch
$S_{3b} = \sqrt{\frac{2}{5}}[\sin\alpha(\Delta r_2 - \Delta r_5) + \sin 2\alpha(\Delta r_3 - \Delta r_4)]$	
$S_{4a} = \sqrt{\frac{2}{5}}[\Delta\alpha_{34} + \cos\alpha(\Delta\alpha_{45} + \Delta\alpha_{23}) + \cos 2\alpha(\Delta\alpha_{15} + \Delta\alpha_{12})]$	asymmetric in plane deformation
$S_{4b} = \sqrt{\frac{2}{5}}[\sin\alpha(\Delta\alpha_{45} - \Delta\alpha_{23}) + \sin 2\alpha(\Delta\alpha_{15} - \Delta\alpha_{12})]$	
$S_{5a} = \sqrt{\frac{2}{5}}[\Delta r_1 + \cos 2\alpha(\Delta r_2 + \Delta r_5) + \cos\alpha(\Delta r_3 + \Delta r_4)]$	asymmetric stretch
$S_{5b} = \sqrt{\frac{2}{5}}[\sin 2\alpha(\Delta r_2 + \Delta r_5) + \sin\alpha(\Delta r_3 + \Delta r_4)]$	
$S_{6a} = \sqrt{\frac{2}{5}}[\Delta\alpha_{34} + \cos 2\alpha(\Delta\alpha_{45} + \Delta\alpha_{23}) + \cos\alpha(\Delta\alpha_{15} + \Delta\alpha_{12})]$	in plane (scissor) deformation
$S_{6b} = \sqrt{\frac{2}{5}}[\sin 2\alpha(\Delta\alpha_{45} - \Delta\alpha_{23}) - \sin\alpha(\Delta\alpha_{15} - \Delta\alpha_{12})]$	
$S_{7a} = \frac{1}{\sqrt{5}}[(\Delta\gamma_{16} - \Delta\gamma_{17}) + \cos 2\alpha(\Delta\gamma_{26} - \Delta\gamma_{27} + \Delta\gamma_{56} - \Delta\gamma_{57}) + \cos\alpha(\Delta\gamma_{36} - \Delta\gamma_{37} + \Delta\gamma_{46} - \Delta\gamma_{47})]$	asymmetric out of plane deformation
$S_{7b} = \frac{1}{\sqrt{5}}[\sin 2\alpha(\Delta\gamma_{26} - \Delta\gamma_{27} - \Delta\gamma_{56} + \Delta\gamma_{57}) - \sin\alpha(\Delta\gamma_{36} - \Delta\gamma_{37} - \Delta\gamma_{46} + \Delta\gamma_{47})]$	

Table VI. G Matrix[a] for Pentagonal Planar XeF_5^- of Symmetry D_{5h}

A_1'	$G_{11} = \mu_y = 5.2637 \times 10^{-2}$
A_2''	$G_{22} = (2/r^2)(\mu_y + 5\mu_x) = 4.4802 \times 10^{-2}$
E_1'	$G_{33} = \mu_y + 5\mu_x/2 = 7.1677 \times 10^{-2}$
	$G_{34} = 5(5^{1/2})\mu_x/(4r \sin\alpha) = 1.1123 \times 10^{-2}$
	$G_{44} = (1/r^2)(5\mu_y \sin^2 2\alpha + \mu_x) = 2.4333 \times 10^{-2}$
E_2'	$G_{55} = \mu_y = 5.2637 \times 10^{-2}$
	$G_{56} = 0$
	$G_{66} = (1/r^2)(4\mu_y \sin^2\alpha) = 4.7026 \times 10^{-2}$
E_2''	$G_{77} = 2\mu_y/r^2 = 2.5995 \times 10^{-2}$

[a] The following geometry was used for the calculation of the G matrix: $r = 2.0124$ Å and $\alpha = 72°$.

had not previously been carried out for such a species. Force constants were calculated by the Wilson FG matrix method.[44] Figure 7 shows our choice of internal coordinates to describe the vibrations of such a molecule. Two imaginary ligands, E_6 and E_7, have been placed in the axial positions to define the angles γ, required for the definition of the out-of-plane deformation modes. The symmetry coordinates and approximate mode descriptions are given in Table V and are derived from those previously reported for the IF_7 molecule after correction for two apparent typographical errors.[45] The analytical G and F matrices, together with the computed numerical values, are given in Tables VI and VII, respectively. The correctness of our G matrix was verified by an independent calculation of the numerical G matrix by using a computational method that gave identical values.

Vibrational Assignments. In agreement with the above predictions for XeF_5^- of symmetry D_{5h}, three mutually exclusive Raman and two infrared bands were observed in the 200–700-cm^{-1} region expected for the fundamental vibrations. The $N(CH_3)_4^+$ salt, containing the largest cation and, hence, the best isolated XeF_5^- anion, shows three narrow Raman lines at 502, 423, and 377 cm^{-1}. On the basis of their relative intensities and frequencies, which are similar to those of the three closely related Raman-active modes of octahedral molecules, the 502-, 423-, and 377-cm^{-1} bands are assigned to the symmetric stretch, $\nu_1(A_1')$, the antisymmetric stretch, $\nu_5(E_2')$, and the symmetric in-plane deformation, $\nu_6(E_2')$, respectively. The rigorous adherence of the observed Raman spectrum to the vibrational selection rules for symmetry D_{5h} and the failure to observe further splittings of the vibrational bands serve to underscore that the vibrational modes of the XeF_5^- anion

(44) Wilson, E. B. *J. Chem. Phys.* **1941**, *9*, 76.
(45) Khanna, R. K. *J. Mol. Spectrosc.* **1962**, *8*, 134.

Table VII. F Matrix and Force Field for Pentagonal Planar XeF_5^- of Symmetry D_{5h}

assignment		freq, cm^{-1}	symmetry force constants[a]
A_1'	ν_1	502	$F_{11} = f_r + 2f_{rr} + 2f_{rr}' = 2.820$
A_2''	ν_2	274	$F_{22} = r^2(f_\gamma + 2f_{\gamma\gamma}\cos\alpha + 2f_{\gamma\gamma}'\cos 2\alpha) = 0.996$
E_1'	ν_3	465	$F_{33} = f_r + 2f_{rr}\cos\alpha + 2f_{rr}'\cos 2\alpha = 1.830$
			$F_{34} = r(f_{r\alpha} + 2f_{r\alpha}'\cos\alpha + 2f_{r\alpha}''\cos 2\alpha) = -0.342$
	ν_4	290	$F_{44} = r^2(f_\alpha + 2f_{\alpha\alpha}\cos\alpha + 2f_{\alpha\alpha}'\cos 2\alpha) = 2.212$
E_2'	ν_5	423	$F_{55} = f_r + 2f_{rr}\cos 2\alpha + 2f_{rr}'\cos\alpha = 2.003$
			$F_{56} = r(f_{r\alpha} + 2f_{r\alpha}'\cos 2\alpha + 2f_{r\alpha}''\cos\alpha) = 0$
	ν_6	377	$F_{66} = r^2(f_\alpha + 2f_{\alpha\alpha}\cos 2\alpha + 2f_{\alpha\alpha}'\cos\alpha) = 1.797$
E_2''	ν_7	79[b]	$F_{77} = r^2(f_\gamma + 2f_{\gamma\gamma}\cos 2\alpha + 2f_{\gamma\gamma}'\cos\alpha) = 0.143$

[a] Stretching constants in mdyn/Å, deformation constants in mdyn Å/rad^2, and stretch–bend interaction constants in mdyn/rad. [b] Value taken from the ab initio calculation.

in its $N(CH_3)_4^+$ salt are only very weakly coupled.[46] It also justifies the use of the assumed free anion symmetry in the subsequent vibrational analysis and force field calculations.

In the salts with smaller cations, stronger coupling of the XeF_5^- motions or slight distortions of the anions can occur, resulting in a splitting of the two E_2' modes into their doubly degenerate components. As expected, the anion–cation interaction is strongest for the NO^+ salt, causing some of the infrared-active modes, such as $\nu_3(E_1')$ and $\nu_4(E_1')$, also to become weakly active in the Raman spectrum.

In the infrared spectra two strong anion bands were observed above 250 cm^{-1}. The first one was a very intense broad band extending from 400 to 550 cm^{-1}, which must be due to the antisymmetric stretching mode $\nu_3(E_1')$. The second one is an intense band at 274 cm^{-1}, which, on the basis of its frequency and relative intensity, must be the symmetric out-of-plane (umbrella) deformation, $\nu_2(A_2'')$.

The third predicted infrared-active mode is the antisymmetric in-plane deformation, $\nu_4(E_1')$. Assuming the F_{66} and F_{44} symmetry force constants to be identical (both modes involve f_α and different combinations of $f_{\alpha\alpha}$ and $f_{\alpha\alpha}'$, with the latter being small due to the large mass of the xenon central atom), a frequency of 274 cm^{-1} was calculated for $\nu_4(E_1')$. Therefore, $\nu_4(E_1')$, which should be of medium infrared intensity, might either be hidden underneath the intense $\nu_2(A_2'')$ band at 274 cm^{-1} or occur just below the 250-cm^{-1} cutoff frequency of the AgBr windows used for our study. A frequency range 240–290 cm^{-1} for $\nu_4(E_1')$ is also supported by the Raman spectrum of $NO^+XeF_5^-$ (see Table IV). In this compound, where the anion–cation interaction is the strongest and the infrared-active modes become also weakly Raman active, two weak Raman bands were observed at 244 and 282 cm^{-1}, respectively. Furthermore, the infrared spectra of $RbXeF_5$ and $CsXeF_5$ exhibit a 288-cm^{-1} shoulder on the strong 275-cm^{-1} band, and the Raman spectra of all the alkali-metal XeF_5^- salts show an extremely weak band at about 290 cm^{-1}. Consequently, a frequency of 290 cm^{-1} was chosen by us for $\nu_4(E_1')$ and used for the force field computations. Our choice of 290 cm^{-1} for ν_4 is also supported by ab initio calculations for XeF_5^- (see below) and IF_7.[47] Assuming the frequency differences between calculated and observed frequencies to be the same for the two in-plane deformation modes in XeF_5^-, a value of 291 cm^{-1} is predicted for ν_4. Similarly, the

(46) A factor-group analysis of the vibrational modes of the unit cell was carried out by use of the correlation chart method (Carter, R. L. *J. Chem. Educ.* **1971**, *48*, 297 and references therein). The free anion symmetry (D_{5h}) was correlated to the site symmetry of the anion (C_s), which, in turn, was correlated to the crystal symmetry (D_{2h}). Assuming complete vibrational coupling occurs in the unit cell of $N(CH_3)_4^+XeF_5^-$, all the vibrational modes of the XeF_5^- anion are found to be Raman- and infrared-active under the crystal symmetry. Moreover, ν_3, ν_4, ν_5, ν_6, and ν_7 will be split into four and three components in their Raman (A_g, B_{1g}, B_{2g}, B_{3g}) and infrared (B_{1u}, B_{2u}, B_{3u}) spectra, respectively; ν_1 will be split into two components in both the Raman (A_g, B_{3g}) and infrared (B_{1u}, B_{2u}) spectra and ν_2 will not be split in the infrared (B_{3u}) but will be split into two components in the Raman (B_{1g}, B_{2g}) spectrum.
(47) Bartell, L. S.; Rothman, M. J.; Gavezzotti, A. *J. Chem. Phys.* **1982**, *76*, 4136 and references cited therein.

Table VIII. Internal Force Constants (mdyn/Å) and Bond Length (Å) of XeF_5^- Compared with Those of XeF_2, XeF_4, and IF_4^-

force const	XeF_2[a]	XeF_4[b]	IF_4^-[b]	XeF_5^-[c]
f_r	2.83	3.055	2.221	2.096
f_{rr}	0.14	0.120	0.183	0.143
f_{rr}'		0.007	0.466	0.219
f_α ($-f_{\alpha\alpha}'$)	0.20	0.193	0.182	0.458
f ($-f'$)		0.299	0.257	0.072
$f_{\alpha\alpha} - f_{\alpha\alpha}'$				0.045
$f_\alpha - f_{\alpha\alpha}$				0.413
$f - f'$				0.093
$f - f$				−0.021
r	1.98	1.953		2.012

[a] Data from ref 53. [b] Data from ref 50. The f values in ref 49 have not been properly normalized and must be divided by two to correspond to the values from this work. [c] This work.

transfer of the computed frequency difference of 102 cm^{-1} for the two in-plane deformation modes from IF_7 to XeF_5^- results in a ν_4 value of 275 cm^{-1} for XeF_5^-.

The only missing fundamental vibration is the ring puckering mode, $\nu_7(E_2'')$, which ideally is inactive in both the infrared and Raman spectra. Since no experimental frequency is available for this mode, the frequency of 79 cm^{-1} obtained by the ab initio calculation (see below) was used.

In addition to the fundamental vibrations, numerous Raman bands were observed in the low-frequency region, which are attributed to lattice vibrations. The infrared spectra exhibit some weak bands above 600 cm^{-1}, which can be readily assigned to different overtones or combination bands of XeF_5^- (see Table IV).

In $NO^+XeF_5^-$ and $N(CH_3)_4^+XeF_5^-$, cation bands were also observed (see Table IV) with frequency values that are in excellent agreement with previous literature data.[4,5,7,48]

Force Constants. The symmetry force constants of XeF_5^- are shown in Table VII. Except for the E_1' and E_2' blocks, all of the symmetry force constants are one-dimensional and well determined. In the two-dimensional E_2' block, G_{56} equals zero (see Table VI), resulting in F_{56} also becoming zero. Therefore, the only remaining underdetermined problem is the two-dimensional E_1' block. The range of possible solutions for this block was computed by using the extremal conditions reported by Sawodny.[49] It has previously been pointed out[49-52] that in weakly coupled (heavy central atom) systems the values of the general valence force field tend to fall within the range given by $F_{34} = 0$ as the lower and $F_{34} = {}^1/_2|F_{34}(\max) - F_{34}(\min)|$ as the upper limit with F_{44} = min being an excellent choice. The latter choice results in an F_{33} value of 1.830 mdyn/Å with an error limit of about 0.14 mdyn/Å and, therefore, F_{33} can be considered to be reasonably well determined.

The most important internal force constants of XeF_5^-, together with the known bond length, are given in Table VIII and are compared with those of the closely related XeF_2[53] and XeF_4[50] molecules and the IF_4^- anion.[50] As can be seen from Table VIII, the force constants well reflect our expectations. Compared with XeF_2 and XeF_4, the increased $^{\delta+}Xe-F^{\delta-}$ polarity of the Xe–F bond in XeF_5^-, combined with the crowding effect in the equatorial plane, should decrease the Xe–F stretching (f_r), increase the in-plane deformation (f_α), and decrease the out-of-plane deformation (f_γ) force constants. Furthermore, ($f_{\alpha\alpha} - f_{\alpha\alpha}'$) and ($f_{\gamma\gamma} - f_{\gamma\gamma}'$) should exhibit positive signs as expected for adjacent angles interacting more strongly than nonadjacent angles. The excellent agreement between these expectations and the experimental values from Table VIII lends strong support to the above assignments for XeF_5^-.

Table IX. Calculated and Experimental Vibrational Frequencies (cm^{-1}) of XeF_4

assignment	calcd freq	obsd freq[a]	approx mode descriptn
A_{1g} ν_1	532	543	ν_{sym} (in phase)
A_{2u} ν_2	271	291	δ_{sym} (out of plane)
B_{1g} ν_3	498	502	ν_{sym} (out of phase)
B_{2g} ν_4	182	235	δ_{sym} (in plane)
B_{2u} ν_5	156	inactive	δ_{asym} (out of plane)
E_u ν_6	591	586	ν_{asym}
E_u ν_7	143	123	δ_{asym} (in plane)

[a] Data from ref 55.

Table X. Calculated and Experimental Vibrational Frequencies (cm^{-1}) for XeF_5^-

	calcd freq			obsd	approx
assignment	*a*	*b*	*c*	freq	mode descriptn
A_1' ν_1	467	537	551	502	ν_{sym} (in plane)
A_2'' ν_2	270	274	275	274	δ_{sym} (out of plane)
E_1' ν_3	502	574	585	400–550	ν_{asym}
E_1' ν_4	248	255	254	290	δ_{asym} (in plane)
E_2' ν_5	413	477	489	423	ν_{asym}
E_2' ν_6	335	356	361	377	δ_{sym} (in plane)
E_2'' ν_7	79	21	28i		δ_{asym} (out of plane)

[a] With the calculated Xe–F bond length of 2.077 Å. [b] With an assumed Xe–F bond length of 2.022 Å. [c] With the observed Xe–F bond length of 2.012 Å.

The data in Table VIII demonstrate that the stretching force constants f_r are mainly influenced by the polarity of the Xe–F bonds, with increasing polarity decreasing the force constant. On the other hand, steric crowding has a strong impact on the deformation constants. If this crowding is anisotropic, as in the case of XeF_5^- where the crowding is concentrated in the equatorial plane, the deformation constants in the congested plane increase while the deformation constants out of the congested plane decrease significantly. The low value of the out-of-plane deformation constant f_γ, in combination with a comparable $f_{\gamma\gamma}$ value, implies a low energy barrier toward puckering of the equatorial plane. When the f_γ value approaches zero or becomes negative, spontaneous puckering should occur.

Computational Results. For a better understanding of the molecular structure of XeF_5^-, local density functional calculations were carried out for this ion and for XeF_4. The quality of these calculations for relatively large and heavy molecules was first tested for the well-characterized[54,55] and closely related XeF_4 molecule. The well-known square-planar (D_{4h}) symmetry and a Xe–F bond length of 1.998 Å (0.045 Å longer than that observed for the solid[54]) were obtained. The calculated vibrational frequencies are in excellent agreement with the experimental values[55] (Table IX), except for the in-plane deformation modes, where the agreement is only fair.

For XeF_5^-, the computations confirmed that the pentagonal planar D_{5h} structure is indeed a minimum. Again, the computed bond length (2.077 Å) is slightly longer (0.065 Å) than the observed one (2.012 Å). A comparison between the observed and calculated spectra is given in Table X. As for XeF_4, the agreement between computed and observed frequencies for XeF_5^- is quite good, with the largest discrepancies again being found for the in-plane deformation modes. These results confirm the assignments made above for XeF_5^-.

The influence of the bond length on the vibrational spectrum of XeF_5^- was also examined by computing the spectra for two shorter Xe–F bond distances, one at the experimental bond length and one 0.01 Å longer (Table X). As expected, the stretching frequencies are the most sensitive to changes in the bond length except for the equatorial ring puckering mode, ν_7, which is also

(48) Christe, K. O.; Wilson, W. W.; Bougon, R. A. *Inorg. Chem.* **1986**, *25*, 2163.
(49) Sawodny, W. *J. Mol. Spectrosc.* **1969**, *30*, 56.
(50) Christe, K. O.; Naumann, D. *Inorg. Chem.* **1973**, *12*, 59.
(51) Pfeiffer, M. *J. Mol. Spectrosc.* **1969**, *21*, 181.
(52) Thakur, S. N.; Rai, S. N. *J. Mol. Struct.* **1970**, *5*, 320.
(53) Siebert, H. *Anwendungen der Schwingungsspektroskopie in der Anorganischen Chemie*; Anorganische und Allgemeine Chemie in Einzeldarstellung, VII; Springer Verlag: Berlin, Germany, 1966.
(54) Burns, J. H.; Agron, P. A.; Levy, H. A. *Science* **1963**, *139*, 1208. Templeton, D. H.; Zalkin, A.; Forrester, J. D.; Williamson, S. M. *J. Am. Chem. Soc.* **1963**, *85*, 242. Ibers, J. A.; Hamilton, W. C. *Science* **1963**, *139*, 106.
(55) Claassen, H. H.; Chernick, C. L.; Malm, J. G. *J. Am. Chem. Soc.* **1963**, *85*, 1927.

Table XI. Valence Molecular Orbitals for XeF_5^-

symmetry	orbital[a]	energy, eV
A_2'	p_y anti on F	3.00
A_2''	p_z anti 0.67 Xe, 0.40 F	3.15
E_1'	p_y on F	3.71
A_1'	0.43 p_x on F, 0.57 s on Xe, anti	4.00
E_2''	p_z on F	4.06
E_1''	p_z on F some Xe d	4.69
E_2'	$p_{x,y}$ on F	4.78
E_2'	$p_{x,y}$ on F	5.72
A_2''	0.77 p_z Xe, 0.21 p_z F	7.38
E_1'	0.56 p_x, p_y Xe, 0.40 p_x on F	9.01
A_1'	0.89 Xe s	16.02

[a] x = Xe–F bond axis, y = orthogonal to Xe–F axis in plane, z = orthogonal to Xe–F axis out of plane.

very sensitive to shortening of the bond length. At the experimental distance, the degenerate deformation frequency becomes imaginary, showing that the molecule would assume a nonplanar structure. As discussed above, increasing congestion in the equatorial ring will result in spontaneous puckering and an imaginary frequency for ν_7. The calculations at the experimental geometry are far enough from the theoretical minimum that the calculated frequencies should be employed only to show the expected trends, as they do not refer to the minimum energy structure. The data in Table X also indicate that the frequency order of the Xe–F stretching modes is essentially independent of the Xe–F bond length. It should be noted that all the calculated frequencies are harmonic values and were not scaled to include anharmonicity effects, which are usually on the order of 5%.

The Mulliken charges for XeF_5^- are +1.48e for the Xe atom and −0.50e for the F atoms. This differs from the nominal assignments of −1.0e for each F and +4.0e for the Xe. The molecular orbitals (Table XI) provide some insight into the bonding in this molecule. If we consider only the valence p orbitals on F since the 2s orbitals are quite low in energy, the remaining orbitals can be qualitatively summed up as follows: There are 10 electrons in the $2p_y$ lone pairs on F orthogonal to the Xe–F bond. There are roughly 10 electrons in the $2p_z$ orbitals on F, which are orthogonal to the molecular plane. The totally symmetric group of these orbitals interacts with the out-of-plane 5p orbital on Xe in a symmetric and antisymmetric way. The $2p_x$ orbitals on fluorine along the Xe–F bond have about 1Oe in them. These mix with the $5p_x$ and $5p_y$ orbitals on Xe. Although the Xe 5s orbital does mix to some extent with the 2p orbitals on F, it is predominantly a lone pair. The basic description is thus a Xe with a $5s^25p_z^2$ occupancy surrounded by five F^- atoms. Delocalization of fluorine electron density into the Xe $5p_{x,y}$ orbitals with only a small participation of the d orbitals on Xe then reduces the charges on the F atoms. The HOMO is the antibonding combination of the in-plane lone pairs on the F atom orthogonal to the Xe–F axis. The NHOMO is almost degenerate in energy with the HOMO and is the antibonding out-of-plane combination of the F $2p_z$ and the Xe $5p_z$ orbitals (Figure 8).

Both the orbitals and the bonding in XeF_5^- are quite similar to those of XeF_4, which were calculated for comparison. In XeF_4, the Mulliken charges on Xe and F are +1.65e and −0.41e, respectively. The Xe 5s orbital participates in two orbitals, with most of its density in the orbital at 22.02 eV just as in XeF_5^-. The $5p_z$ orbital of Xe and the out-of-plane $2p_z$ orbitals on the fluorines interact to give bonding and antibonding molecular orbitals. The orbital configuration at Xe is thus dominated by the $5s^25p_z^2$ configuration just as in the anion. The HOMO in XeF_4 is at 9.15 eV and is the $5p_y$ antibonding orbital as found in XeF_5^-. Its significantly higher value, compared with that of XeF_5^-, is in agreement with our expectations for an anion and its parent molecule.

It is important to note that the calculations provide a molecular orbital description of the bonding in XeF_5^- and XeF_4. The orbitals reported above are the canonical orbitals with molecular symmetry. Because of the molecular symmetry, the 5s and $5p_z$ orbitals cannot mix and thus give separate s^2 and p^2 occupancies. In contrast,

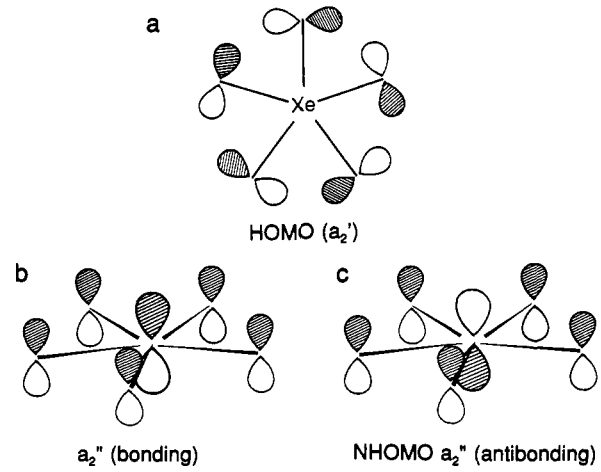

Figure 8. Selected molecular orbitals for XeF_5^-. (a) HOMO, antibonding combination of in-plane p_y's on F; (b) bonding out-of-plane orbital combination between Xe $5p_z$ and p_z's on F; (c) antibonding out-of-plane orbital combination between Xe $5p_z$ and p_z's on F.

in the VSEPR model used elsewhere in this work, the valence electron lone pairs may be described as two doubly occupied sp hybrids above and below the plane, but this is not required by the VSEPR model. The two models are equivalent, as the VSEPR model is derived from a localized orbital approach, whereas the calculations are based on a molecular orbital approach. The sum and difference of the $5s^2$ and $5p_z^2$ orbitals will lead to the two sp hybrid lone pairs. However, the total electron density, which is the invariant quantity, is independent of the choice of models used to describe it. (In a formal sense, the wave function is invariant to a unitary transformation.)

Conclusions

Xenon tetrafluoride indeed forms stable adducts with strong Lewis bases, such as tetramethylammonium fluoride and the heavier alkali-metal fluorides. However, contrary to previous reports,[13-15] these salts do not contain the XeF_6^{2-} dianion, but the XeF_5^- anion.

The XeF_5^- anion has a highly unusual pentagonal planar structure for which no other examples were previously known. It can be derived from that of a pentagonal bipyramid, such as IF_7,[38] in which the two axial fluorine ligands have been replaced by two sterically active free valence electron pairs. Compared with IF_7,

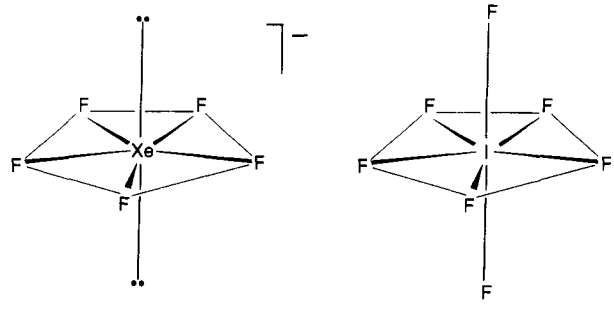

which is a fluxional molecule undergoing with relative ease a dynamic ring-puckering pseudorotation,[38,47] the equatorial XeF_5 plane of XeF_5^- appears to be considerably more rigid. The increased rigidity of the XF_5 plane in XeF_5^- is attributed to the stabilizing effect of the two free valence electron pairs on xenon. These free pairs are more diffuse and hence more repulsive than the axial I–F bond pairs in IF_7, thereby offering more resistance toward the puckering of the equatorial XeF_5 plane.

Acknowledgment. We thank C. J. Schack, W. W. Wilson, R. D. Wilson, and S. S. Tsai for their help; F. Adar, Instruments S.A.; Edison, NJ, for recording the single-crystal Raman spectrum of $N(CH_3)_4^+XeF_5^-$; the U.S. Air Force Astronautics Laboratory, Edwards AFB (K.O.C. and G.J.S.); the U.S. Army Research Office (K.O.C.) and the Natural Sciences and Engineering Re-

search Council of Canada (G.J.S.) for financial support; Ministry of Foreign Affairs, France, for a Lavoisier Fellowship (H.P.M.); and C.N.R.S. Laboratoire des Agrégats Moléculaires et Matériaux Inorganiques, Montpellier, France, for granting a leave of absence to H.P.M.

Supplementary Material Available: Tables of anisotropic thermal parameters (Table 1) and hydrogen atomic coordinates (Table 2) (2 pages); tabulation of calculated and observed structure factor amplitudes (Table 3) (13 pages). Ordering information is given on any current masthead page.

Thermodynamics and Kinetics of Carbon Dioxide Binding to Two Stereoisomers of a Cobalt(I) Macrocycle in Aqueous Solution

Carol Creutz,* Harold A. Schwarz,* James F. Wishart, Etsuko Fujita, and Norman Sutin

Contribution from the Chemistry Department, Brookhaven National Laboratory, Upton, New York 11973. *Received October 1, 1991*

Abstract: The thermodynamics and kinetics of binding of CO_2, CO, and H^+ to *N*-racemic and *N*-meso stereoisomers of the cobalt(I) macrocycle CoL^+ (L = 5,7,7,12,14,14-hexamethyl-1,4,8,11-tetraazacyclotetradeca-4,11-diene) have been determined in aqueous media with use of the pulse radiolysis technique and transient ultraviolet–visible spectroscopy. *N-rac*- or *N-meso*-CoL^+ was produced by the hydrated electron reduction of *N-rac*- or *N-meso*-CoL^{2+}, with *tert*-butyl alcohol generally added to scavenge hydroxyl radicals. Reactions of both *N-rac*- and *N-meso* CoL^+ are readily followed by the disappearance of intense (ϵ 1 × 10^4 M^{-1} cm^{-1}) absorption bands at 630 and 635 nm, respectively. The product absorptions are much less intense (ϵ 200–500 M^{-1} cm^{-1}) and shifted to higher energy (400–500 nm). Carbon dioxide adducts were also produced via the reactions of *N-rac*- or *N-meso*-CoL^{2+} with formate radical $^{\bullet}CO_2^-$ in solutions containing sodium formate and CO_2 and hydrogen ion adducts (hydrides) by the reactions with $^{\bullet}H$ atom in acid solution. The known stereochemistry of the methyl radical additions to *N-rac*- and *N-meso*-CoL^{2+} was used to assign the different isomers of the adducts. Thus, reaction of $^{\bullet}H$ and $^{\bullet}CO_2^-$ with *N-rac*-CoL^{2+} yields *sec-N-rac*-$CoL(H)^{2+}$ and *sec-N-rac*-$CoL(CO_2)^+$, respectively, and the reaction of *N-rac*-CoL^+ with H^+ and CO_2 yields *prim-N-rac*-$CoL(H)^{2+}$ and *prim-N-rac*-$CoL(CO_2)^+$, respectively. As expected, only *N*-meso adducts are obtained from either *N-meso*-CoL^+ or *N-meso*-CoL^{2+}. Formation constants for the complexes (determined by analysis of equilibrium absorptions or equilibration kinetics) at 25 °C are $CoL(CO_2)^+$, 2.5 × 10^8 M^{-1} (prim-*N*-rac), 6.0 × 10^6 M^{-1} (*N*-meso); $CoL(CO)^+$, 1.6 × 10^8 M^{-1} (prim-*N*-rac), 0.8 × 10^8 M^{-1} (*N*-meso); $CoL(H)^{2+}$, 2.5 × 10^{11} M^{-1} (prim-*N*-rac), ≥7.9 × 10^{13} M^{-1} (*N*-meso). The rate constants are large and generally parallel the stability of the adduct. The following are values of k (M^{-1} s^{-1}) for addition at 25 °C: CO_2, 1.7 × 10^8 (prim-*N*-rac), 1.5 × 10^7 (*N*-meso); CO, 5.0 × 10^8 (prim-*N*-rac), 8.3 × 10^8 (*N*-meso); H^+, 3.0 × 10^9 (prim-*N*-rac), 2.3 × 10^9 (*N*-meso).

Introduction

Cobalt complexes have attracted attention as potential catalysts for photo- and electroreduction of water to H_2 and of carbon dioxide to CO and HCO_2^-.[1-5] The cobalt(I) complexes, which are accessible through photo- or electroinduced one-electron reduction of the cobalt(II) complexes, may bind hydrogen ion or carbon dioxide and, in some cases, facilitate their reduction. A particularly attractive family for systematic studies is the tetraazacyclotetradecyl macrocycle series,[6] in which the cobalt(II)/(I) potential ranges from −0.34 to −1.65 V (versus SCE) in acetonitrile.[7] In such a series, the relationships between metal reduction potentials, ligand steric factors, etc. and the reactivity of the complex toward both the binding and reduction of small molecules may be explored. Indeed, this problem is currently being studied by several groups.[7-10]

Of the above series, the macrocycle L = 5,7,7,12,14,14-$(CH_3)_6$-1,4,8,11-tetraazacyclotetradeca-4,11-diene has received the most intensive study to date. For this ligand, the Co(III)/(II) and Co(II)/(I) reduction potentials are ca. −0.2 and −1.34 V, respectively, vs SCE in acetonitrile.[7] The cobalt(III) complexes are six-coordinate, the low-spin d^7 cobalt(II) complexes appear to be five- or six-coordinate, and the low-spin d^8 cobalt(I) complexes are four- or five-coordinate.[11,12] Stereoisomers of the complexes arise through the chirality of the saturated nitrogen atoms.[13] Although *cis*-Co(III)LB (B = bidentate ligand) is known, most complexes of this series are trans, with the four nitrogen atoms of the macrocycle occupying the equatorial plane of the complex. At minimum, two trans isomers (*N*-meso and *N*-racemic) are possible. In aqueous solutions of the five- or

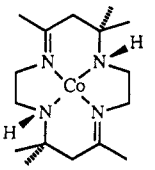

N-rac L

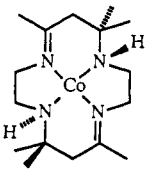

N-meso L

six-coordinate CoL^{2+} (the coordination sphere of the cobalt(II) being completed by solvent molecule(s)), the *N*-rac isomer is favored at equilibrium but the *N*-meso isomer can also be studied in pH <7 solutions.[12] The low-spin d^8 CoL^+ can also exist as either isomer, as will be seen. When the axial positions of the complex are asymmetrically substituted (CoLXY, X and Y different ligands), three isomers are possible—*N*-meso, primary *N*-rac, and

(1) Brown, G. M.; Brunschwig, B. S.; Creutz, C.; Endicott, J. F.; Sutin, N. *J. Am. Chem. Soc.* **1979**, *101*, 1298-1300.
(2) Fisher, B.; Eisenberg, R. *J. Am. Chem. Soc.* **1980**, *102*, 7363-7366.
(3) Pearce, D. J.; Pletcher, D. *J. Electroanal. Chem.* **1986**, *197*, 317.
(4) Simpson, T. C.; Durand, R. R. *Electrochim. Acta* **1988**, *33*, 581.
(5) Tinnemans, A. H. A.; Koster, T. P. M.; Thewissen, D. M. W. H.; Mackor, A. **1984**, *103*, 288.
(6) Tait, A. M.; Lovecchio, F. V.; Busch, D. H. *Inorg. Chem.* **1977**, *16*, 2206.
(7) Fujita, E.; Creutz, C.; Sutin, N.; Szalda, D. J. *J. Am. Chem. Soc.* **1991**, *113*, 343-353.
(8) Gangi, D. A.; Durand, R. R. *Chem. Soc., Chem. Commun.* **1986**, 697.
(9) Creutz, C.; Schwarz, H. A.; Wishart, J. F.; Fujita, E.; Sutin, N. *J. Am. Chem. Soc.* **1989**, *111*, 1153-4.
(10) Schmidt, M. H.; Miskelly, G. M.; Lewis, N. S. *J. Am. Chem. Soc.* **1990**, *112*, 3420-3426.
(11) Szalda, D. J.; Fujita, E.; Creutz, C. *Inorg. Chem.* **1989**, *28*, 1446-50.
(12) Szalda, D. J.; Schwarz, C. L.; Endicott, J. F.; Fujita, E.; Creutz, C. *Inorg. Chem.* **1989**, *28*, 3214-19.
(13) Warner, L. G.; Rose, N. J.; Busch, D. H. *J. Am. Chem. Soc.* **1968**, *90*, 6938-6946.

0002-7863/91/1513-3361$02.50/0